The tip of the manipulator thus reaches a maximum velocity of 3 m/s and acceleration of 3.8 g. The joint trajectory error has a peak of 0.4° and an average error of 0.055°. This result is competitive with previous tracking data of direct-drive robots where model-based feedforward techniques were used. Thus, the proposed control system design along with proper arm design provides a simple solution to the complex problem of high-speed trajectory following.

## V. Conclusion

This paper demonstrates that, through arm mechanism design, the work of designing controllers for high-speed trajectory tracking can be simplified. The experimentally determined system transfer function provided an accurate system model that was used in controller design. The decoupled dynamics and invariant inertia of the M.I.T. direct-drive arm led to the design of an invariant feedforward-type controller that performed pole/zero cancellation to the plant dynamics. The experimental results show that the proposed controller enabled the arm to follow 2- and 5-Hz command signals accurately with a 0.055° mean trajectory error. This tracking performance is achieved with high-speed maneuvers: an end point maximum speed of 3.0 m/s and a maximum acceleration of 3.8 g. In addition, the accuracy of one joint is independent of the other joints' motions.

## References


[1] C. An, C. Atkeson, and J. Hollerbach, "Experimental determination of the effect of feedforward control on the trajectory of tracking errors," in *Proc. IEEE Conf. Robotics Automat.*, Apr. 1986.

[2] H. Asada, T. Kanade, and I. Takeyama, "Control of a direct-drive arm," *ASME J. Dynam. Syst., Meas., Contr.*, vol. 105, no. 3, pp. 136–142, 1983.

[3] H. Asada and K. Youcef-Toumi, "Analysis and design of semi-direct-drive robot arms," in *Proc. Amer. Contr. Conf.*, (San Francisco), 1983, pp. 757–764.

[4] ——, "Analysis and design of a direct-drive arm with a five-bar-link parallel drive mechanism," *ASME J. Dynam. Syst., Meas. Contr.*, vol. 106, no. 3, pp. 225–230, 1984.

[5] ——, "Decoupling of manipulator inertia tensor by mass redistribution," in *Proc. ASME Mechan. Conf.*, Oct. 1984.

[6] ——, *Direct-Drive Robots - Theory and Practice*. Cambridge, MA: MIT Press, June 1987.

[7] P. Khosla and T. Kanade, "Real-time implementation and evaluation of model-based controls on CMU DD Arm II," in *Proc. IEEE Conf. Robotics Automat.* Apr. 1986.

[8] L. Ljung and T. Soderstrom, *Theory and Practice of Recursive Identification*. Cambridge, MA: MIT Press, 1983.

[9] H. Schwartz, "A recursive identification controller for the trajectory tracking of mechanical systems," Doctor of Philosophy dissertation, Mechanical Eng. Dept., Massachusetts Institute of Technology, Feb. 1987.

[10] P. Turner and H. A. Pak, "Optimal tracking controller design for invariant dynamics direct-drive arms,"*ASME J. Dynam. Syst., Meas. Contr.*, vol. 108, pp. 360–365, 1986.

[11] K. Youcef-Toumi, "Analysis, design and control of direct-drive manipulators," Doctor of Science dissertation, Mechanical Eng. Dept., Massachusetts Institute of Technology, May 1985.

[12] K. Youcef-Toumi and H. Asada, "Dynamic decoupling and control of a direct-drive manipulator," in *Proc. IEEE Conf. Decision Contr.*, Dec. 1985.

[13] ——, "The design of open-loop manipulator arms with decoupled and configuration-invariant inertia tensors," *ASME J. Dynam. Syst., Meas. Contr.*, vol. 109, Sept. 1987.

[14] K. Youcef-Toumi and A. T. Y. Kuo, "Dynamic decoupling and control of a direct-drive manipulator," in *Proc. IEEE Conf. Decision Contr.*, Dec. 1987.


# A Torque Sensing Technique for Robots with Harmonic Drives

Minoru Hashimoto, Yoshihide Kiyosawa, and Richard P. Paul

***Abstract*—We propose a joint torque sensing technique making use of the existing structural elasticity of robots. The technique provides joint torque sensing without reducing the stiffness of the robot or changing the mechanical structure of the joints. The elasticity of the flexsplines of the harmonic drives is utilized to measure the joint torque. The flexsplines are flexible thin cups, made from steel, in the harmonic drives that are driven by the wave generators. In this paper, we perform a finite-element analysis of the flexsplines that shows that a special configuration of strain gauges, mounted on the flexspline, has to be employed to eliminate errors in sensor information due to rotation of the wave generator. Characteristics of the torque sensor are then examined experimentally. The linearity and the dynamic response are almost the same as those of a conventional sensing technique. Joint torque control, using the proposed sensor, is implemented for a one-link robot arm. Both theoretical and experimental investigations support the validity of the proposed sensing technique.**

## I. Introduction

Joint torque information has been considered useful to improve robot control:

- Since a joint torque servo, using a joint torque sensor, is closed around each joint and does not contain the variable link inertia of a robot, a high-bandwidth torque inner loop can be implemented in robot force control [1]–[3].
- Disturbance torques caused by reducers and actuators, such as wedging action between the two mating teeth in reducers, friction losses in drive trains, and ripple torques of actuators, can be compensated by the joint torque feedback control. Thus, the joint torque control improves the accuracy of robot motion control [4].
- We can measure the effect of outer links on a joint, including nonlinear dynamic interactions between links, by the joint torque sensor. Dynamic control of robots can then be performed by joint torque sensing without the need to compute the inverse dynamics of the robot [5]–[7].

In order to apply these control schemes to actual robots, joint torque sensors have been developed. In the conventional technique, strain gauges are cemented on the output shaft of the motor reducer [1], [2]. Recently, Pfeffer *et al.* proposed joint torque sensing for a PUMA 500 [4]. The sensor has been placed between a bull gear and a link, replacing the standard attachment bolts with flexures instrumented with strain gauges. The technique they described, however, requires changing the mechanical structure of the joints to introduce compliant members into the manipulator.

On the other hand, many robots already have structural flexibility in the drive system. The torsional elasticity in the drive system imposes bandwidth limitations on any control algorithm. Algorithms that are designed assuming perfect rigidity may cause stability problems by

Manuscript received September 6, 1990; revised June 2, 1992. Portions of this paper were presented at the IEEE International Conference on Robotics and Automation, Scottsdale, AZ, May 14–19, 1989.

M. Hashimoto is with the Department of Mechanical Engineering, Kagoshima University, 1-21-40 Korimoto, Kagoshima 890, Japan.

Y. Kiyosawa is with Harmonic Drive Systems Inc., 4034 Toyoshina, Toyoshina-machi Minamiazumi-gun, Nagano-ken 399-82, Japan.

R. P. Paul is with the Department of Computer and Information Science, University of Pennsylvania, Philadelphia, PA 19104.

IEEE Log Number 9205081.

1042-296X/93$03.00 © 1993 IEEE

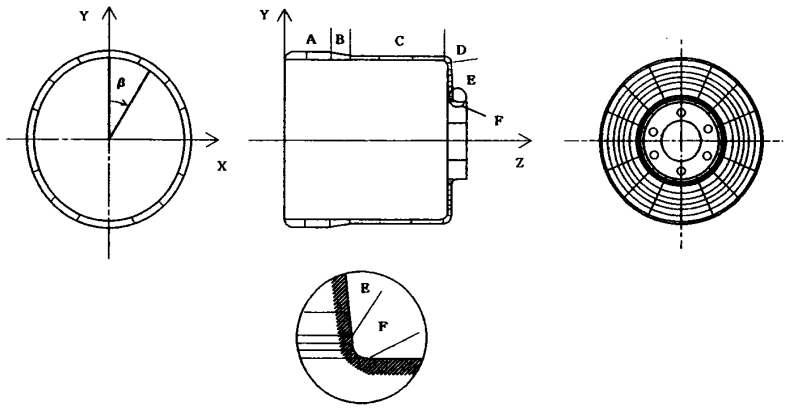


Fig. 1. Element segmentation of the flexspline.

neglecting the joint flexibility [3], [8]. However, the joint elasticity may be effectively used for sensing joint torques; we do not have to add any additional compliant members or change the mechanical structure to measure the joint torques. This sensing technique can be used to improve the control performance to correct problems introduced by the flexibility of the robot joint gear reducer [9]–[11].

In this paper, we employ the elasticity in a harmonic drive itself to measure the joint torque. The technique provides joint torque sensing without reducing stiffness of the robot or changing the mechanical structure of the joint. Harmonic drives are widely used as reducers for robots. A harmonic drive system is a compact, high-torque, high-ratio, in-line gear mechanism incorporating a rigid "circular spline," an elliptical "wave generator" and a nonrigid "flexspline." The flexspline is a flexible thin cup made of steel. Elasticity of the flexspline could be utilized to obtain the joint torque information, since the torque at a joint axis, not the actuator axis, is transmitted through the flexspline. The open end of the flexspline is deformed elliptically by the wave generator connected to the motor shaft. It is thus difficult to find a way to measure the actual torque transmitted with strain gauges [7], [12]. The purpose of this paper is to show how we can measure the joint torques, utilizing joint elasticity itself, based on theoretical and experimental studies.

In Section II, a finite-element analysis of flexsplines is used to investigate shear strains on flexsplines under loaded and unloaded conditions. We then show how to eliminate changes in sensor information due to wave generator rotations. In Section III, a joint torque sensing technique with a special configuration of strain gauges is proposed, based on theoretical analysis of the flexspline. The characteristics of the proposed sensor are examined experimentally by comparing it with a conventional torque sensor. In Section IV, the dynamics and joint torque control using the sensor are shown to demonstrate the validity of the sensor.

## II. Finite-Element Analysis of Flexsplines

To study the torsional stiffness of the harmonic drive, deformations of flexsplines under torque-loaded conditions have been investigated [13]. In this section, we examine strains on the flexspline from the point of view of torque sensing. We used 3-D thick shells with 16 nodes in the finite-element analysis [14]. The flexspline was segmented with 256 elements as shown in Fig. 1. Global and local coordinates were used in the computation, and the stiffness matrix was computed using the local coordinate system. The flexspline opening is deformed elliptically by forced displacements at the opening's upper and lower ends. The bottom of the flexspline is fixed, and torsional strains caused by loaded torques are applied on the circumference of a circle at the opening. The flexspline parts, shown in Fig. 1, are: the teeth, $A$; the cylindrical part, $C$; and the radial part, $E$. $\beta$ is the angle from the longer axis of the ellipse in the opening part. Strains are computed at four integral points in each element. Since we need shear strain information for torque sensing, we compute strains along two directions rotated $\pi/4$ and $3\pi/4$ about the normal axis of the element plane. These two strains are then subtracted from each other to obtain a shear strain. We have measured of flexsplines made by Harmonic Drive Systems Inc.[1]

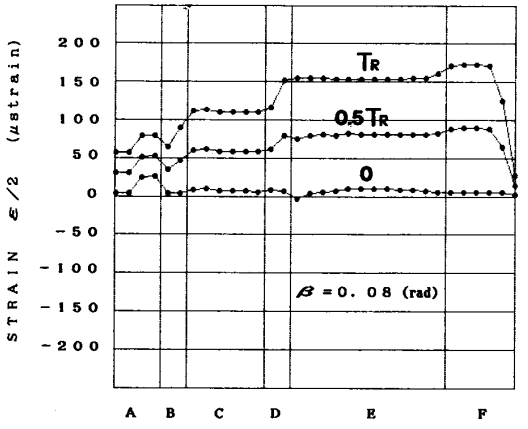


Fig. 2. Axial analysis of shear strains on a flexspline.

### A. Strain Analysis along the Axis Direction

A 49-mm-diameter flexspline was used to make this analysis. Shear strains were computed as a function of axial positions with a circular angle $\beta = 0.08$ rad (Fig. 2). In Fig. 2, positions on the flexspline are indicated by letters of the alphabet. The half values of shear strains are plotted on the ordinate. The values of loaded torques were: 0, $0.5T_R$, and $T_R$, where $T_R$ is the rated torque of the flexspline.

A suitable position for the strain gauges to measure joint torque is at a place where there is linearity in the relation between shear strain and loaded torque, and where shear strain does not depend on axial position. The points $B$, $D$, and $F$ are not acceptable positions,

[1] Harmonic Drive is a registered trade name in Japan, the Republic of Korea, and the Republic of China.

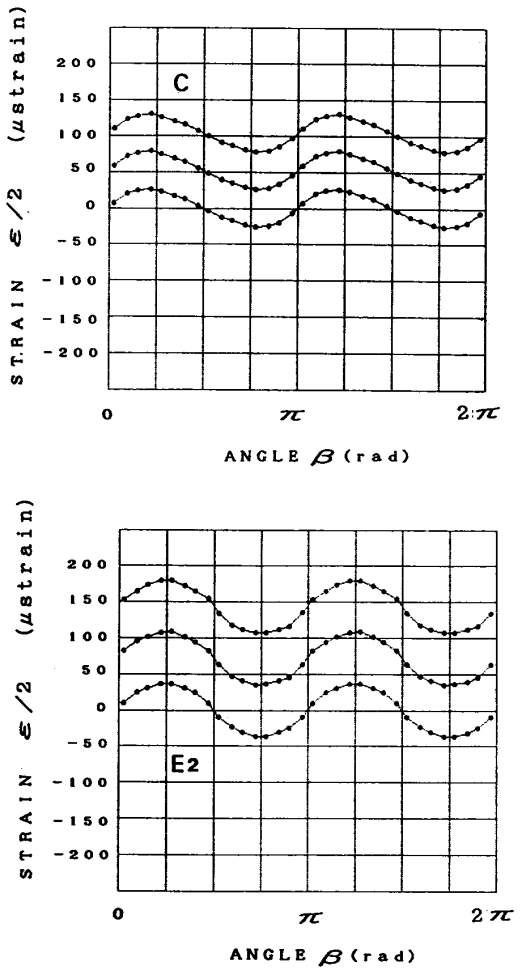


Fig. 3. Circular analysis of shear strains on a flexspline.

since at these points shear strain depends on axial position. It is impossible to put strain gauges on part $A$, because the inner and outer sides of the part come into contact with the wave generator and the circular spline. Based on these considerations, points $C$ and $E$ are appropriate as gauge positions to measure torsional strains on the flexspline. Points $C$ and $E$ are cylindrical and radial locations, respectively, as shown in Fig. 1.

### *B. Strain Analysis along the Circumference Direction*

Fig. 3 shows the computational results of shear strain as a function of circular angle $\beta$ of the flexspline. Point $C$ is shown on the left, and point $E$ on the right. There are periodic modulations in shear strains that do not depend on applied torques. These changes are caused by an elliptical deformation (see Fig. 4). We must remove this modulation to obtain actual torque information. To do this, we introduce the additional strain curve $\tilde{A}$ shown in Fig. 4. By adding the other curve $\tilde{A}$, whose phase is shifted a half wavelength from the original curve $A$, the modulation could be eliminated. Curve $\tilde{A}$ of shear strains can be obtained at a position shifted $\pi/2$ in circular angle $\beta$ from that of curve $A$. This technique is applied to modulations on the cylindrical and the radial parts. The results are shown in Fig. 5. The change of the shear strains on the radial part has been, for the most part, eliminated by the technique. The remaining oscillation on

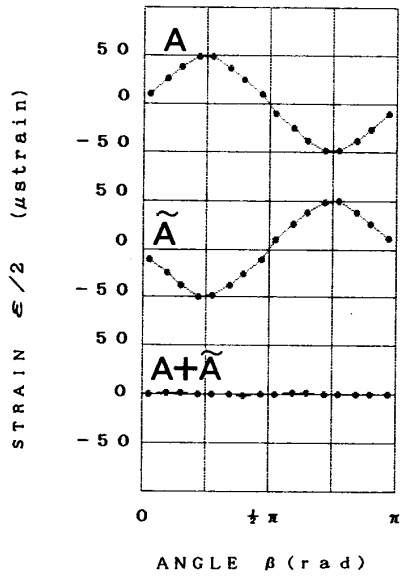


Fig. 4. Elimination of changes in strains.

the cylindrical part is caused by the fact that curves $A$ and $\tilde{A}$ on the part are not exactly sinusoidal. The curves on both cylindrical and radial parts change almost linearly with torque. However, the shear strain on the radial part is greater than that of the cylindrical part under the same torque load. The radial part is, therefore, suitable as a place where strain gauges may be located, based on accuracy and sensitivity considerations.

### *C. Torsional Stiffness of Flexsplines*

Since the proposed technique employs the elasticity of the flexsplines, the sensitivity of torque sensing depends on the torsional stiffness of flexsplines. It is important to know the torsional stiffness of the flexsplines as a function of the harmonic drive size. The shear strain per unit torque is plotted in Fig. 6 as a function of the flexspline diameter. The values of shear strain decrease rapidly with the diameter of the flexspline. The bigger the flexspline, the less sensitive it is to applied torques. However, the applied torques increase with an increase of the flexspline diameter. Fig. 7 shows the change of flexspline rated torques. We compute the shear strain when the rated torque is applied for each flexspline (Fig. 8). The shear strain on the flexspline under the rated torque is from 100 to 300 $\mu$strain. Thus, by using strain gauges, we can measure the shear strain of every flexspline with good sensitivity.

## III. Joint Torque Sensing Technique

In order to measure shear strain, two gauges are cemented on positions $R1$ and $R2$; see Fig. 9(a). Fig. 9(a) shows the strain gauge configuration on a radial part. The two gauges are placed along the directions of $\pi/4$ and $3\pi/4$ about the bottom circle's center line. Strains $\epsilon 1$ and $\epsilon 2$ on gauges R1 and R2 are described by the following equations.

$$\epsilon_1 = \epsilon_t + \epsilon_w \tag{1}$$

$$\epsilon_2 = -\epsilon_t + \epsilon_{w'} \tag{2}$$

where $\epsilon_t$ and $\epsilon_w$ are the strains caused by the applied torque and by the deformation due to the wave generator, respectively. The difference between the strains, $\epsilon_1 - \epsilon_2$, results in the shear strain

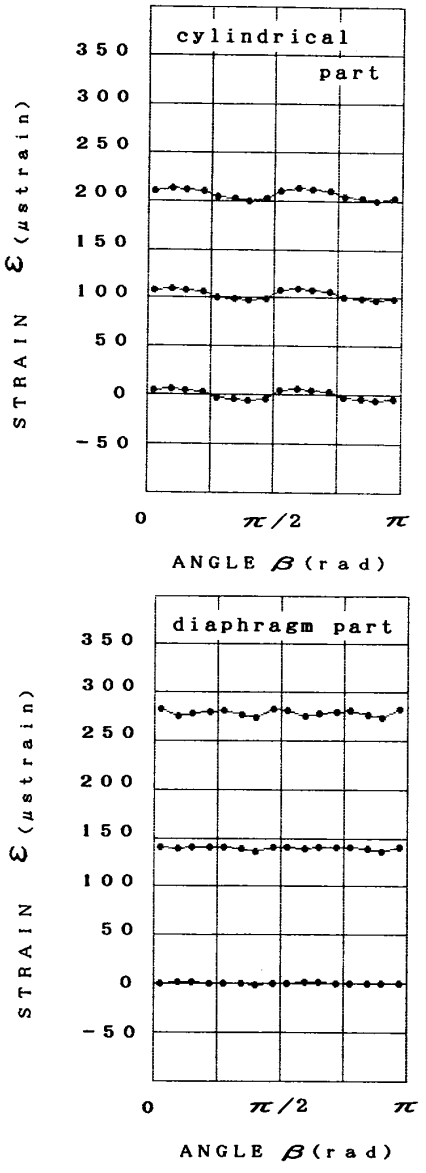


Fig. 5. Shear strains generated by applied torques.

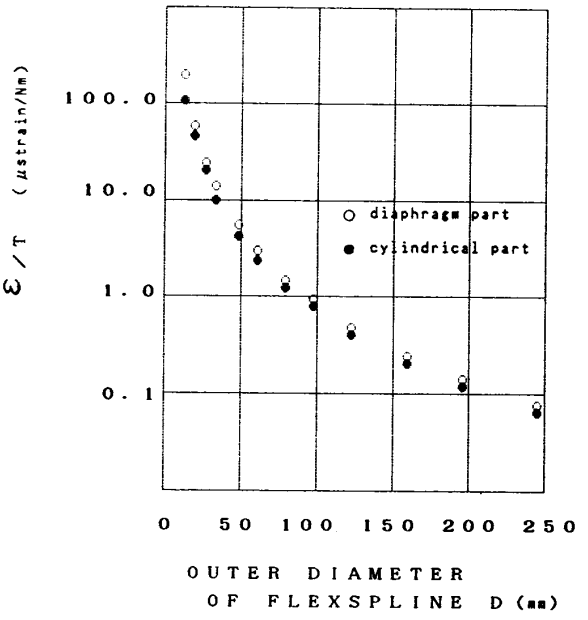


Fig. 6. Flexibility of flexsplines.

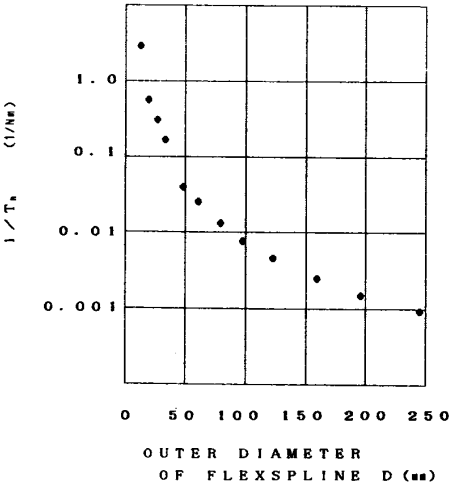


Fig. 7. Rated torques for various flexsplines.

information. According to the curves in Fig. 3, the difference can be written as

$$\epsilon_1 - \epsilon_2 = 2\epsilon_t + \Psi_0 \sin(2\beta) \tag{3}$$

where we assume the modulation curves of $\epsilon_{w} - \epsilon_{w'}$ are sinusoidal. In order to cancel the modulation $\Psi_0 \sin(2\beta)$ and to detect the actual torsional strain $\epsilon_t$, we need an additional signal $\tilde{A}$, as mentioned in Section II. The two active gauges located at positions R3 and R4 in Fig. 9(a) generate signal $\tilde{A}$ . Positions R3 and R4 are situated on the position rotating $\pi/2$ from positions R1 and R2 on the center of the bottom, respectively. Signal $\tilde{A}$ is obtained by the difference of strains $\epsilon_3$ and $\epsilon_4$ on position R3/R4.

$$\epsilon_3 - \epsilon_4 = 2\epsilon_t + \Psi_0 \sin(2\beta - \pi). \tag{4}$$

If a Wheatstone bridge is constructed with the four active gauges R1–R4, the output voltage is described by

$$\begin{aligned} E_{\text{output}} &= \frac{K_{gf}}{4}(\epsilon_1 + \epsilon_3 - \epsilon_2 - \epsilon_4)E_{\text{supply}} \\ &= K_{gf}\epsilon_t E_{\text{supply}} \end{aligned} \tag{5}$$

where $K_{gf}$ is a gauge factor of the gauges. $E_{\text{supply}}$ and $E_{\text{output}}$ denote input and output voltages, respectively, to the Wheatstone bridge. The temperature compensation is performed at the same time in the strain gauge bridge. In Fig. 9, four optional gauges R5–R8 are introduced to maintain symmetry with R1–R4.

The voltage resolution in this sensor is defined by

$$K_R = \frac{E_{\text{output}}}{T} \tag{6}$$

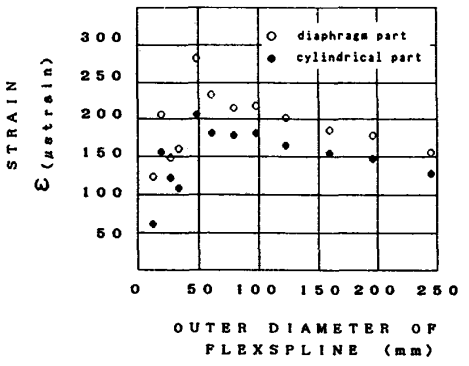


Fig. 8. Shear strains on flexsplines under rated torques.

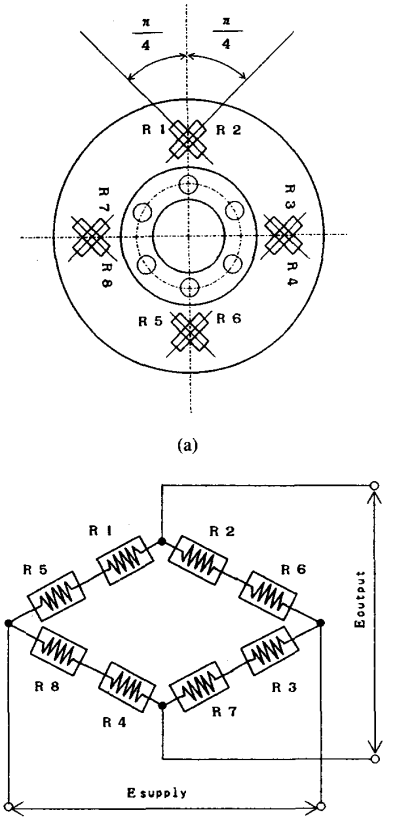


Fig. 9. A strain gauge configuration and the Wheatstone bridge for joint torque sensing.

where $T$ is an applied torque. On the radial part, the strain caused by torque $T$ can be obtained analytically (see the Appendix) by

$$\epsilon_t = \frac{T(r_1 + r_2)}{8\pi t G r_1^2 r_2} \tag{7}$$

where $G$ is the shearing modulus of the material. $t$ is the thickness of the radial part. $r_1$ and $r_2$ are radiuses of the fixed part and the diaphragm, respectively. By combining (5), (6), and (7), we can compute the resolved torque gain as

$$K_R = \frac{K_{gf} E_{\text{supply}}(r_1 + r_2)}{8\pi t G r_1^2 r_2}. \tag{8}$$

### A. Sensing Inaccuracy Due to Gauge Position Error

It is important to locate the strain gauges at exact positions. In practice, however, this is impossible, and the position errors of the strain gauges will generate sensing errors. We will discuss sensing inaccuracy due to the circumferential error of gauge locations. As shown in Fig. 2, a radial deviation in gauge position does not cause much change of the sensor output. On the other hand, a circumferential deviation could be serious. If we denote the relative angular deviation $\Delta\alpha$ between gauge positions R1/R2 and R3/R4, (4) must be rewritten as

$$\begin{aligned}\epsilon_3 - \epsilon_4 &= 2\epsilon_t + \Psi_0 \sin\left\{2\left(\beta - \frac{\pi}{2} - \Delta\alpha\right)\right\} \\ &= 2\epsilon_t - \Psi_0 \sin\{2(\beta - \Delta\alpha)\}.\end{aligned} \tag{9}$$

By adding (3) to (9) and modifying it, we obtain

$$\epsilon_1 + \epsilon_3 - \epsilon_2 - \epsilon_4 = 4\epsilon_t + \Psi \sin(2\beta + \gamma) \tag{10}$$

where

$$\gamma = \tan^{-1}\left\{\frac{\sin 2\Delta\alpha}{1 - \cos 2\Delta\alpha}\right\} \tag{11}$$

$$\Psi = 2\Psi_0 |\sin \Delta\alpha|. \tag{12}$$

Hence, the magnitude of the inaccuracy due to the gauge position deviation is proportional to the amplitudes of the original signal, either $A$ or $\dot{A}$.

To evaluate the sensing inaccuracy, we use an index

$$E_R = \frac{\Psi}{4\epsilon_t^R} = \frac{\Psi_0 |\sin \Delta\alpha|}{2\epsilon_t^R} \tag{13}$$

where $\epsilon_t^R$ is the torsional strain under the rated torque. Therefore, it is important to know the relative values of amplitude $\Psi_0$ to the rated torque. We compute amplitude $\Psi_0$ as a function of the flexspline size using the finite-element method described in Section II. The flexspline diameter used in the computations are 13, 49, 98, and 245 mm. In the simulated results, the magnitudes of $\Psi_0$ did not depend on the flexspline sizes; instead, $\Psi_0 = 100$ $\mu$strain. Since the values of $\epsilon_t^R$ are about 200 $\mu$strain for almost all flexsplines, as shown in Fig. 7, the value $E_R$ does not change much with the size of the flexsplines, $E_R = 0.25|\sin \Delta\alpha|$. It is reasonable to evaluate the inaccuracy for angular errors $\Delta\alpha$ within $\pm 2°$. In this case, the sensing inaccuracy $E_R$ due to the angular error is approximately within $\pm 1\%$ of the rated torque.

### B. Characteristics of the Proposed Sensor

As shown Fig. 10, there are two types of harmonic drive. In the case of Type A, the flexspline is fixed on the casing, and the circular spline is connected with the output shaft. Type B is the opposite of Type A with the output shaft connected to the flexspline and the circular spline connected to the stationary casing. The cables of the strain gauges rotate with the joint rotation in Type B. However, the rotation of the cables does not cause any problem in practice. This is because joints in robots do not usually rotate over one revolution and the gauges rotate with the joint, not the actuator. We can therefore apply the proposed sensing technique to both types of harmonic drive.

An experimental system, shown in Fig. 11, is utilized to examine characteristics of the proposed sensor. We employ a Type A harmonic drive that has a reduction ratio of 1:101. The rated torque of the harmonic drive is about 40 N·m. The flexspline diameter is 49 mm.

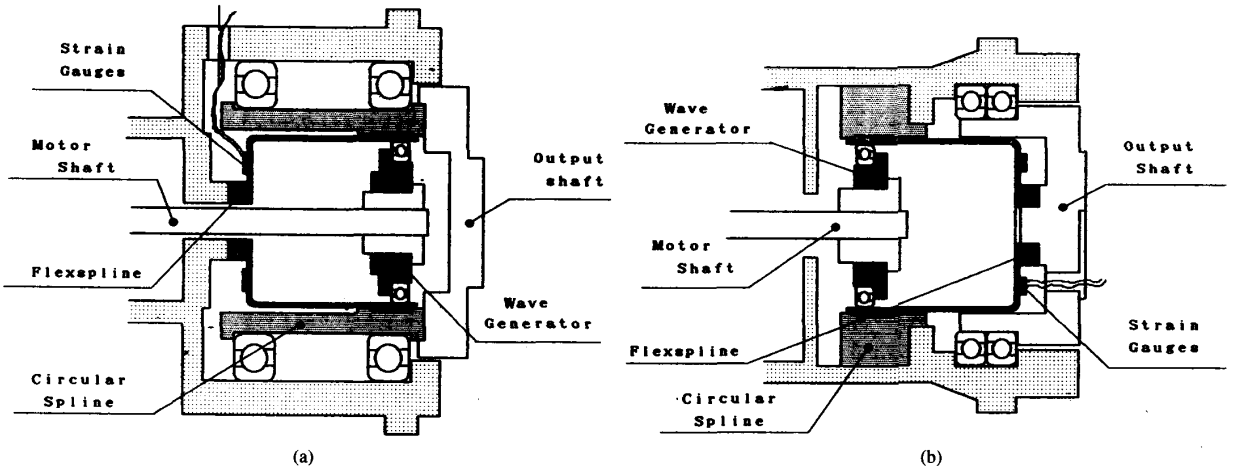


Fig. 10. Schematic drawing of harmonic drives.

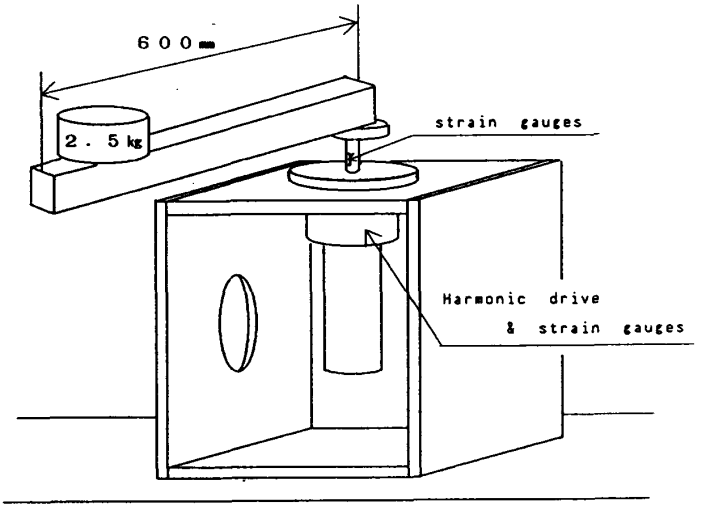


Fig. 11. Schematic drawing of an experimental system.

The link is made from an aluminum alloy, and the length is 600 mm. A weight is set at the link tip with a mass of 2.5 kg. In order to compare the proposed technique with a conventional one, an elastic shaft was also mounted between the link and the harmonic drive, and torques on the shaft were measured (see [1] and [2]). A 37-W dc motor is used as an actuator. We mounted eight strain gauges with 120 $\Omega$ on the radial part of the flexspline as shown in Fig. 9(a). The strain gauges are made from Cu-Ni alloy foil and have a gauge factor $K_{gf} = 2.1$. The gauge-grid length is 1 mm. The gauges are connected to form a balanced Wheatstone bridge as shown in Fig. 9(b). The input voltage $E_{\text{supply}}$ is 3 V. The measurements of the radial part of the flexspline are $t = 0.39$ mm, $r_1 = 15.8$ mm and $r_2 = 24.85$ mm. The voltage resolution of this sensor is obtained by (8) as

$$K_R = 50\ \mu\text{V/N·m} \tag{14}$$

where $G = 8.3 \times 10^{10}\ \text{N/m}^2$ for Ni-Cr-Mo steel, which is the material used for the flexsplines. The bridge output signal is amplified by a factor of 500. The sensed output voltage sensitivity is 25 mV/N·m.

The linearity and hysteresis in the sensor were measured. Torques were applied to the output shaft of the flexspline with the wave generator immobilizing by a brake. The proposed sensor has good linearity without hysteresis (Fig. 12). The sensitivity of the proposed sensor is 24 mV/N·m, which is close to the theoretical result obtained earlier. The link was immobilized to examine the dynamical response of the sensor. A rectangular-pulse voltage was applied to the motor. Fig. 13 shows the results of the sensor output. The difference between the outputs of the proposed sensor and the conventional one is shown in Fig. 13. The responses of the proposed and conventional sensors are the same. In order to investigate sensor characteristics during motion of the arm, the step response in the joint angle was investigated using a position control law (Fig. 14). The observed error between the sensor outputs is very small. The proposed sensor output follows that of the conventional sensor even when the joint rotates. From those experiments, we can conclude that the torque sensor on the flexspline is a useful joint torque sensor for robot manipulators.

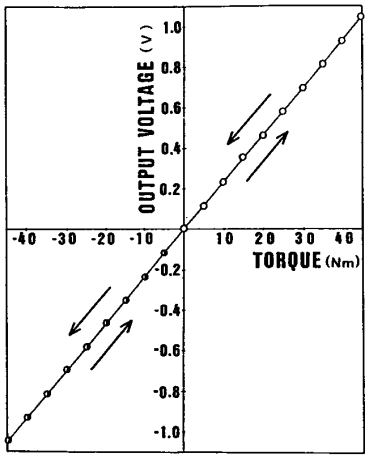


Fig. 12. Linearity and hysteresis in the proposed sensor output.

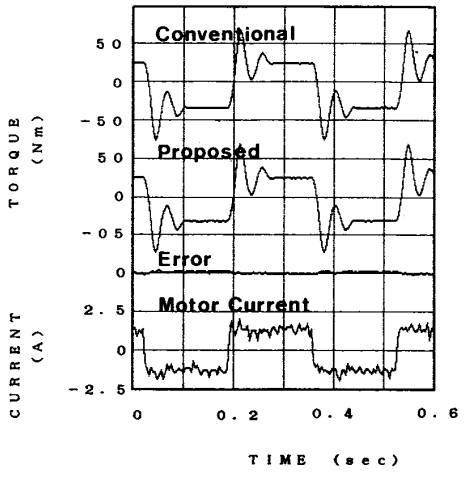


Fig. 13. Dynamic responses of the proposed and conventional sensors.

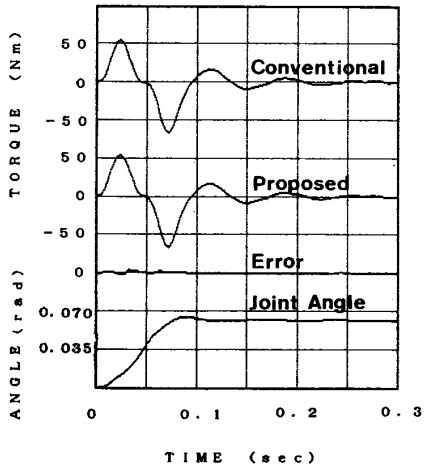


Fig. 14. Sensor outputs during a joint motion.

## IV. Joint Torque Control

When end-point force control is implemented, high-gain feedback will produce instability because the robot structure is inherently a low-bandwidth flexible system and the force sensor is situated at the end of this structure. This bandwidth limitation can be reduced by joint torque control, since joint torque sensors are situated before the low-bandwidth robot structure [3], [8].

We have applied joint torque control, using the proposed torque sensor, to a one-link arm with a harmonic drive. The dynamics of the drive system can be modeled by

$$J_L\ddot{q}_L - K\left(\frac{q_M}{N} - q_L\right) = 0 \tag{15}$$

$$NJ_M\ddot{q}_M + K\left(\frac{q_M}{N} - q_L\right) + N\tau_F = N\tau_M \tag{16}$$

$$T_J = K\left(\frac{q_M}{N} - q_L\right) \tag{17}$$

where $q_L$ and $q_M$ represent the link angles and motor angles, respectively. $K$ is the joint stiffness. $J_L$ and $J_M$ are the link inertia and the rotor inertia, respectively, $\tau_M$ is the torque applied by the motor, and $N$ is the gear reduction ratio. $\tau_F$ is Coulomb friction at the drive system. We idealized the system by assuming large joint stiffness and small joint damping, neglecting altogether the damping terms. According to (15)–(17), we can rewrite the dynamic equation as

$$N\tau_M = N^2J_MK^{-1}\ddot{T}_J + T_J + N\tau_F + N^2J_MJ_L^{-1}T_J. \tag{18}$$

We selected the following control scheme. It combines feedforward compensation with joint torque feedback to provide a high reduction of disturbances and robustness to model error.

$$N\tau_M = N^2J_MK^{-1}\left\{\ddot{T}_d + K_d\left(\dot{T}_d - \dot{T}_J\right) + K_p(T_d - T_J)\right\} + T_d\left(1 + N^2J_MJ_L^{-1}\right). \tag{19}$$

In this control law, we design the dynamic response by selecting values for $K_p$ and $K_d$. The steady-state torque error caused by Coulomb friction is

$$E_T = \frac{N\tau_F}{\left(N^2J_MK^{-1}K_p + 1 + N^2J_MJ_L^{-1}\right)}. \tag{20}$$

An experimental system, shown in Fig. 11, was utilized to examine the characteristics of torque feedback control. The elastic shaft for conventional torque sensing was removed, and we only used the harmonic-drive built-in torque sensor. In this experimental system, we employed a Type B harmonic drive with a reduction ratio of 1:100. A digital signal processor, $\mu$PD 77230, has been used for the servo controller. The sampling period of the torque servo is 0.5 ms. The achievable gain $K_p$ is limited by the digital-controller sampling frequency. In the case of a 0.5-ms sampling period, gains $K_p$ and $K_d$ of 46 808 and 234 s were selected for this experiment. The parameters of the experimental system are listed in Table I. The experiments were performed under the constrained link condition. When the link is immobilized, the equations can be found by considering the limit as the inertia becomes infinite.

Fig. 15 shows the static characteristics of the open-loop and the closed-loop systems. The result of the open-loop system shows a hysteresis loop. The magnitude of the hysteresis loss is about $\pm 4$ N·m. The hysteresis loss is 10% of the rated torque of the harmonic drive. When torque feedback control is implemented, the width of the hysteresis is greatly reduced.

The step response is improved by torque feedback control as shown in Fig. 16. The result of open-loop control shows a steady-state error of 70%. In the case of the closed-loop system, the steady-state error is almost zero. The 10–90% rise time for the closed-loop system is approximately 7 ms.

TABLE I
PARAMETERS OF THE EXPERIMENTAL SYSTEM

| Parameters | Values |
|---|---|
| Link Inertia $J_L$ | 0.88 kg$^2$ |
| Rotor Inertia $J_M$ | 0.000 094 kg$^2$ |
| Joint Stiffness $K$ | 8800 N·m/rad |
| Torque Constant $K_t$ | 0.1 N·m/V |
| Reduction Ratio $N$ | 100 |

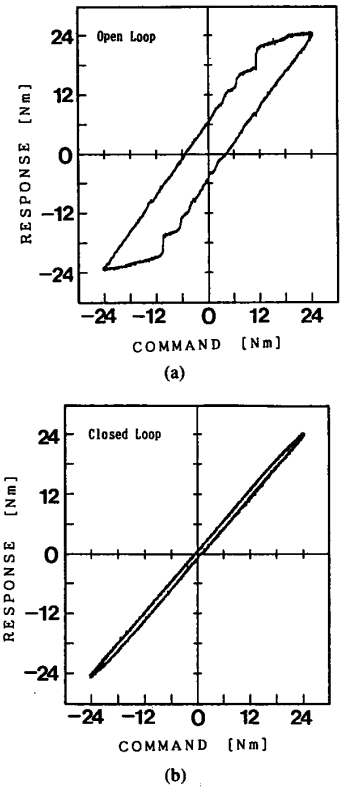


Fig. 15. Static characteristic of torque control. Torque (a) open-loop and (b) closed-loop response.

The experimental frequency response, conducted at a desired amplitude of 5 N·m and a frequency of 20 Hz, is shown in Fig. 17. The tracking error and the dynamic response are much improved by torque closed-loop control. In the open-loop case, the response has very poor performance. The response when the joint torque feedback is included, and it shows good tracking performance.

## V. CONCLUSIONS

Based on theoretical and experimental studies, we have proposed a joint torque sensing technique that makes use of harmonic-drive elasticity. It has been shown that we can eliminate the changes in sensed data, due to wave generator rotations, by using a special strain gauge configuration. By means of finite-element analysis, we found that the stiffness of flexsplines is suitable for torque sensing, as their deformation under normal operating conditions is appropriate for measuring strains for each harmonic drive. We also determined that the optimal location for placing gauges is on the radial part of flexsplines. To verify our sensing technique, a single joint arm with

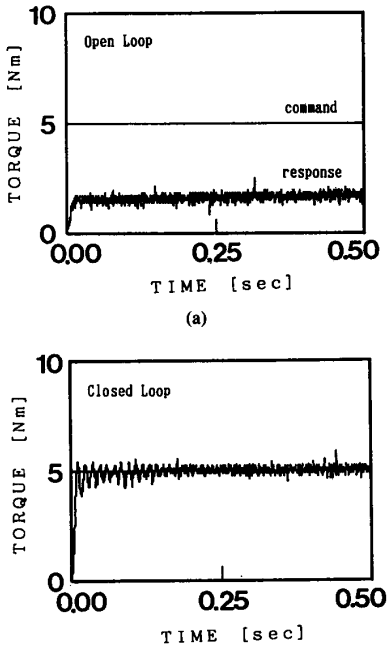


Fig. 16. Step response in torque control. Torque (a) open-loop and (b) closed-loop response.

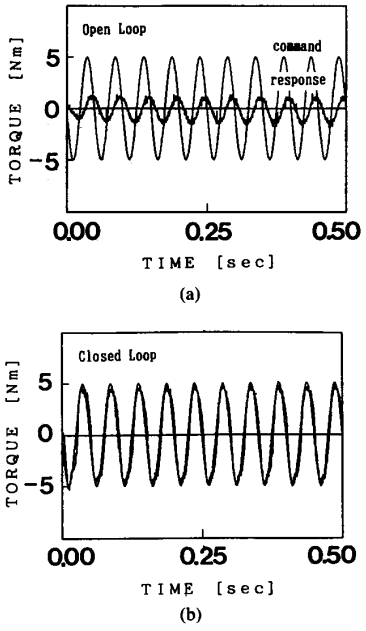


Fig. 17. Frequency response in torque control. Torque (a) open-loop and (b) closed-loop response.

our sensor and a conventional sensor was built. The results show that the characteristics of the proposed sensor are almost the same as those of the conventional technique. Furthermore, joint torque control using the proposed sensor results in excellent performance. Improved sensitivity in torque sensing and in noncontact sensing techniques will be undertaken in future research.

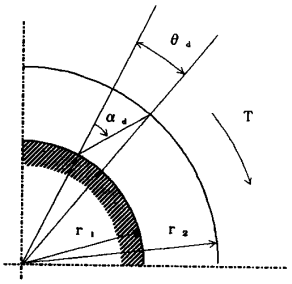


Fig. 18. Modeling of a radial part on flexsplines.

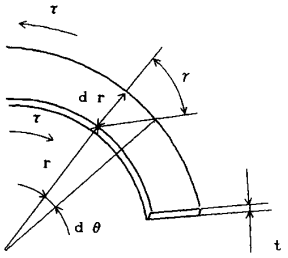


Fig. 19. A small element on a radial part.

Our technique does not require the introduction of additional elasticity into robots to measure joint torques; such changes would degrade and change the mechanical structure of the robot. The range of applications of the proposed sensor are left as the subject of future research.

## APPENDIX

To obtain an equation of strain on a radial part, we model the part as a disk whose inner and outer radiuses are $r_1$ and $r_2$, respectively (Fig. 18). The inside of the disk is fixed, and a torque is applied on the outside. Consider a small element on the disk situated on radius $r$ as shown Fig. 19. The shear stress $\tau$ acting on the small part is described by

$$\tau = \frac{T}{2\pi r^2 t} \tag{A1}$$

where $T$ is an applied torque and $t$ is the thickness of the disk. The shear strain $\gamma$ is, therefore,

$$\gamma = \frac{\tau}{G}. \tag{A2}$$

Then

$$d\theta = \frac{\gamma dr}{r} = \frac{T}{2\pi r^3 tG} dr. \tag{A3}$$

From the relation of Fig. 15 and (A3)

$$\theta_d = \int_{r_1}^{r_2} d\theta = \frac{T}{4\pi tG}\left(\frac{1}{r_1^2} - \frac{1}{r_2^2}\right) \tag{A4}$$

while

$$\alpha_d = \frac{r_2}{(r_1 - r_2)}\theta_d. \tag{A5}$$

If the gauges are mounted on the part at $\pi/4$ and $3\pi/4$, then the sensed strains $\epsilon_t$ caused by torque $T$ are

$$\epsilon_t = \frac{\alpha_d}{2} = \frac{T}{8\pi tG}\left(\frac{1}{r_1^2} - \frac{1}{r_2^2}\right)\frac{r_2}{r_1 - r_2}. \tag{A6}$$

## ACKNOWLEDGMENT

The authors would like to thank K. Fukuda, T. Shimono, H. Hirabayashi, and N. Takizawa for their technical assistance and advice. They would also like to acknowledge Prof. H. Zhang of the University of Alberta for his helpful suggestions and a critical reading of the manuscript.

## REFERENCES

[1] C. Wu and R. Paul, "Manipulator compliance based on joint torque control," in *Proc. 19th IEEE Conf. Decision Contr.* (Albuquerque, NM), vol. 1, Dec. 1980, pp. 88–94.
[2] J. Luh, W. Fisher, and R. Paul, "Joint torque control by a direct feedback for industrial robots," *IEEE Trans. Automat. Contr.*, vol. AC-28, no. 2, pp. 153–161, 1983.
[3] C. H. An and J. M. Hollerbach, "Dynamic stability issues in force control of manipulators," in *Proc. IEEE Int. Conf. Robotics Automat.* (Raleigh, NC), May 1987, pp. 890–896.
[4] L. E. Pfeffer, O. Khatib, and J. Hake, "Joint torque sensory feedback in the control of a PUMA manipulator," *IEEE Trans. Robotics Automat.*, vol. 5, no. 4, pp. 418–425, 1989.
[5] M. Vukobratovic, D. Stokic, and N. Kircanski, *Non-Adaptive and Adaptive Control of Manipulation Robots, Scientific Fundamentals of Robotics 5.* New York: Springer-Verlag, 1985, pp. 152–154.
[6] K. Kosuge, H. Takeuchi, and K. Furuta, "Motion control of a robot arm using joint torque sensors," in *Proc. CDC, 27th Conf. Decision Contr.* (Austin, TX), Dec. 7–9, 1988.
[7] M. Hashimoto, "Robot motion control based on joint torque sensing," in *Proc. IEEE Int. Conf. Robotics Automat.* (Scottsdale, AZ), May 1989, pp. 256–261.
[8] S. D. Eppinger and W. P. Seering, "Understanding bandwidth limitations in robot force control," in *Proc. IEEE Int. Conf. Robotics Automat.* (Raleigh, NC), Apr. 1987, pp. 904–909.
[9] L. M. Sweet and M. C. Good, "Redefinition of the robot motion-control problem," *IEEE Contr. Syst. Mag.*, pp. 18–25, Aug. 1985.
[10] T. Hidaka, T. Ishida, Y. Zhang, M. Sasahara, and Y. Tanioka, "Vibration of a strain wave gearing in an industrial robot," in *Proc. Int. Power Transm. Gearing Conf. New Technol. Power Transm. 90*, 1989, pp. 789–794.
[11] T. Marilier and J. A. Richard, "Nonlinear mechanic and electric behavior for a robot axis with a harmonic drive gear," *Robotics Comput. Integrated Mfg.*, vol. 5, no. 2–3, pp. 129–136, 1989.
[12] M. Hashimoto, Y. Kiyosawa, R. P. Paul, and H. Hirabayashi, "A joint torque sensing technique for robots with harmonic drives," in *Proc. IEEE Int. Conf. Robotics Automat.* (Sacramento, CA), Apr. 1991, pp. 1034–1039.
[13] S. Yanabe, S. Ishizuka, T. Yamaguchi, and M. Ikeda, "Torsional stiffness of harmonic drive reducers," *Trans. Japan Soc. Mechanic. Eng.*, part C, vol. 55, no. 509, pp. 216–221, 1989 (in Japanese).
[14] O. C. Zienkiewicz, *The Finite Element Method in Engineering Science.* Maidenhead, Berkshire, England: McGraw-Hill House, 1971.